

Active Particle Destabilize Passive Membranes

David A. King^{1, 2, *} Thomas P. Russell^{3, 1} and Ahmad K. Omar^{1, 2, †}

¹Materials Science Division, Lawrence Berkeley National Laboratory, Berkeley CA 94720.

²Department of Materials Science and Engineering, University of California, Berkeley, CA 94720.

³Polymer Science and Engineering Department, University of Massachusetts, Amherst MA 01003.

We present a theory for the interaction between active particles and a passive flexible membrane. By explicitly solving for the pressure exerted by the active particles, we show that they *reduce* the membrane tension and bending modulus and introduce novel *non-local* contributions to the membrane mechanics. This theory predicts activity-induced instabilities and their morphology are in agreement with recent experimental and simulation data.

Cells are intrinsically active systems, maintained far from equilibrium by continuous energy consumption. Two hallmark behaviors, reproduction by mitosis and feeding by phagocytosis, require major morphological manipulations mediated by active cytoskeletal forces on the cell membrane [1–4]. Understanding how localized active stresses induce large-scale deformations in flexible membranes is key to unraveling these processes.

Recently, synthetic model systems, such as vesicles loaded with bacteria [5], Janus colloids [6] or magnetic rollers [7], have allowed the interplay between active mechanics and membrane response to be examined. Through interactions with the active particles, the vesicles can exhibit non-equilibrium fluctuation spectra [5] and extreme shape instabilities [6], including division [7].

In this Letter, we present a theoretical framework to describe these instabilities. As a canonical example, we consider spherical active Brownian particles (ABPs) with radius b confined to one side of an infinite membrane. This geometry is appropriate for exceedingly large vesicles and enables analytical progress while capturing the essential physics. By explicitly solving for the pressure exerted by ABPs on the fluctuating membrane, we show that their influence can be captured by renormalizing the membrane's physical properties: they introduce *non-local interactions* and can *reduce* both the surface tension and the bending modulus. Crucially, when these effective parameters become negative, a membrane *stable* in equilibrium can undergo an *activity-induced instability*, the qualitative thresholds and morphology of which agree well with recent simulations and experiments.

We begin with the dynamics of a passive, impermeable membrane interacting with a suspension, active or passive [8, 9]. The membrane is immersed in a d -dimensional solvent and is flat at rest (a line in $d = 2$ or a plane in $d = 3$ with no spontaneous curvature). The normal coordinate to the flat membrane is z , and \mathbf{x} denotes the $(d - 1)$ coordinates along it. Deviations from flat are described by the height function $h(\mathbf{x}, t)$ [10].

The suspension occupies $z \geq h(\mathbf{x}, t)$ and exerts a pressure on the membrane that depends on its internal me-

chanics and how the two are coupled. Our goal is to understand how this interaction affects the membrane's dynamics in the overdamped (no inertia) and linear (small deviation $|\nabla h| \ll 1$) limit, governed by [11]:

$$\partial_t \tilde{h}(\mathbf{q}, t) = \tilde{M}(\mathbf{q}) \left[\tilde{\xi}(\mathbf{q}, t) - \delta \mathcal{H} / \delta \tilde{h}(\mathbf{q}, t) - \tilde{P}(\mathbf{q}, t) \right]. \quad (1)$$

Here, $\tilde{h}(\mathbf{q}) = \int d\mathbf{x} e^{i\mathbf{q} \cdot \mathbf{x}} h(\mathbf{x})$, denotes the Fourier transform (FT) in \mathbf{x} and introduces the wave vector \mathbf{q} . The left-hand side is the FT of the membrane's local z -velocity. Energy dissipation as the membrane moves through the solvent gives rise to the mobility, $\tilde{M}(\mathbf{q})$, which is the FT of the zz -component of the Oseen tensor if hydrodynamic interactions between the suspension and membrane are ignored [12–15]. The bracketed terms on the right-hand side are the non-dissipative, $\hat{\mathbf{z}}$ -directed forces per unit $(d - 1)$ -dimensional area on the membrane: The first, $\tilde{\xi}$, represents thermal fluctuations as a Gaussian, zero-mean, temporally white noise satisfying the fluctuation-dissipation theorem. The second encodes the membrane's internal mechanics through the standard Helfrich Hamiltonian $\mathcal{H} = \int d\mathbf{q} (\gamma q^2 + \kappa q^4) \tilde{h}^2 / 2$ [16, 17], where $q = |\mathbf{q}|$, γ is the surface tension and κ is the bending modulus. The final term is the pressure exerted by the suspension (in FT) which, if the particle-membrane interactions are short-ranged contact forces, is: $P(\mathbf{x}, t) = -\hat{\mathbf{n}} \cdot \boldsymbol{\sigma}(\mathbf{x}, z = h(\mathbf{x}, t)) \cdot \hat{\mathbf{n}}$ [14], where $\boldsymbol{\sigma}$ is the suspension stress and $\hat{\mathbf{n}} = (\hat{\mathbf{z}} - \nabla h) / (1 + |\nabla h|^2)^{1/2}$ is the membrane normal [10, 18].

Takatori and Sahu used Eq. (1) to study non-equilibrium fluctuations of vesicles loaded with bacteria [5]. However, instead of deriving P from the stress tensor, they modeled it as an athermal stochastic variable caused by bacteria-membrane collisions. This captured the experimentally observed fluctuation spectrum scaling $\sim q^{-4}$ as $q \rightarrow 0$ (the equilibrium scaling is q^{-2} [19]) but *cannot* predict activity induced instabilities of otherwise stable membranes, because P was assumed to be independent of h . From Eq. (1), this implies h always fluctuates around the stable minimum, $h = 0$. The pressure from a passive *ideal* gas is independent of h , but this is generally not the case [20–24]. ABPs, ideal or interacting, are known to accumulate, and exert more pressure, on valleys in a boundary than its hills [25–32]. Intuitively, this can lead to an instability for flexible mem-

* daking2@lbl.gov

† aomar@berkeley.edu

branes: the excess pressure grows the valleys, drawing in more active particles to grow them further. This mechanism has qualitatively described instabilities in flexible filaments [32, 33]. Here, we develop a quantitative theory to understand activity induced membrane instabilities.

The key quantity is the suspension stress at the membrane surface. For a general overdamped suspension, this is found from the mechanical force balance: $\nabla \cdot \boldsymbol{\sigma} + \mathbf{b} = \mathbf{0}$, where \mathbf{b} are the body forces. We consider a system of ABPs acted on by: a Brownian force resulting in translational diffusion with constant $D_T = k_B T / \zeta$, where ζ is the translational drag coefficient associated with the solvent drag force, a fixed propulsion force ζv_0 , where v_0 is the “swim speed”, in a direction $\hat{\mathbf{u}}$ that undergoes rotational diffusion with re-orientation time $\tau_r = D_r^{-1}$, and conservative, pairwise, repulsive inter-particle forces. Mechanical balance in this case gives [34]

$$\nabla \cdot \boldsymbol{\sigma} + \mathbf{F} - \zeta \mathbf{J}_\rho = \mathbf{0}, \quad (2)$$

where \mathbf{J}_ρ is the number density current. The non-conservative active and drag force densities appear as the body forces, $\mathbf{F} = \zeta v_0 \mathbf{m}$ and $\zeta \mathbf{J}_\rho$ respectively, where \mathbf{m} is the polarization (the local average of $\hat{\mathbf{u}}$). The Brownian (ideal-gas) and conservative inter-particle forces contribute to $\boldsymbol{\sigma}$ [35–37]. The force exerted by the membrane enforces no-flux at its surface.

Generally, $\boldsymbol{\sigma}$ includes contributions from density gradients. However, when $\ell_0/b \gtrsim 1$ where $\ell_0 = v_0 \tau_r$ is the ABP “run length”, these are negligible in comparison to similar terms appearing in \mathbf{F} [34], allowing $\boldsymbol{\sigma}$ to be approximated by the “conservative pressure”: $\boldsymbol{\sigma} \approx -P_c(\rho) \mathbf{I}$, where \mathbf{I} is the identity. Here, P_c is specified by an “equation of state” that depends only on ρ , and may be obtained from simulations in the absence of a microscopic theory [38]. In the non-interacting limit, $P_c \rightarrow k_B T \rho$, while at the maximum packing density, ρ_{\max} , it diverges. The pressure exerted by the ABPs on the membrane is $P(\mathbf{x}, t) = P_c(\mathbf{x}, z = h(\mathbf{x}, t), t)$, and is solely determined by the local density of active particles in contact with membrane. On small length scales, this should be treated as a stochastic variable, as suggested in Ref. [5]. However, we focus on large-scale deformations driven by *many* ABPs that are better handled using a coarse-grained, deterministic description. While this prevents us from accurately describing the membrane’s fluctuation spectrum, we can determine its stability, which is controlled by the deterministic terms in Eq. (1).

The mechanical balance Eq. (2) makes it clear that to determine the surface density we must understand *both* the complete density field, ρ , and the polarization \mathbf{m} . Each are governed by a continuity equation:

$$\partial_t \rho = -\nabla \cdot \mathbf{J}_\rho, \quad \text{and} \quad \partial_t \mathbf{m} = -(d-1) D_r \mathbf{m} - \nabla \cdot \mathbf{J}_m. \quad (3)$$

The sink $\propto \mathbf{m}$ in the second represents relaxation due to rotational diffusion, the constitutive equation for \mathbf{J}_ρ is given by Eq. (2) and \mathbf{J}_m is the polarization current, for which we use the following phenomenological equation

that may be motivated from microscopic principles [34]:

$$\mathbf{J}_m = -D_T \nabla \mathbf{m} + v_0 \rho \mathcal{V}(\rho) \mathbf{I} / d. \quad (4)$$

This neglects the nematic order of the ABPs, a good approximation outside *rigid* walls with long-wavelength variations ($q \gtrsim b^{-1}$) [29, 30], and supposes inter-particle interactions can be accounted for through $\mathcal{V}(\rho)$, representing the dimensionless local average ABP swim speed. At low densities or in the absence of interactions, they swim freely: $\mathcal{V} \rightarrow 1$. At high densities they are trapped: $\mathcal{V}(\rho_{\max}) \rightarrow 0$. The second term in Eq. (4) leads to an “active pressure”, $P_{\text{act}}(\rho) = \zeta \ell_0 v_0 \rho \mathcal{V}(\rho) / [d(d-1)] = k_B T \alpha^2 \rho \mathcal{V}(\rho)$, due to forces generated by the particles’ swimming, whose scale is set by both their density and activity [37, 39], defined here by: $\alpha = \ell_0 / \Lambda_d [d(d-1)^2]^{-1/2}$, where $\Lambda_d = [D_T \tau_r / (d-1)]^{1/2}$ is the “diffusion length”.

It is well known that above certain activities and densities, homogeneous interacting ABP suspensions undergo “Motility Induced Phase Separation” (MIPS) into regions of high and low density [40]. ABPs also accumulate at walls, potentially rendering a suspension stable at bulk density ρ_∞ unstable near the boundary. We assess the onset of MIPS using the mechanical *spinodal* criterion $P_c(\rho) + P_{\text{act}}(\rho) \leq 0$ (dots denote ρ derivatives), identifying the linear instability of the homogeneous suspension [34]. Understanding the response of a membrane interacting with phase separating ABPs, including nucleation that can occur *between* the spinodal and binodal, is a rich but complicated problem. We focus on suspensions that are linearly stable everywhere, including at the wall-enhanced density [41] and neglect nucleation, while still finding interesting behavior.

Equations (1–4) are closed, involving h , ρ and \mathbf{m} *only*, but are non-linear and difficult to solve analytically. To proceed, we make an additional approximation based on the separation of timescales between ABP relaxation and that of low-tension membranes. From Eqs. (1) & (3), a membrane perturbation with $q \ll b$ relaxes at a rate $\propto q^3$ when $\gamma \approx 0$, while it relaxes more rapidly in the ABP density, $\propto q^2$. This suggests an “adiabatic approximation”: at each instant, the ABPs are assumed to be in steady state with the membrane profile. A finite surface tension requires α to be sufficiently large for this to hold, and it will describe wavenumbers in the range $\alpha^{-2} \lesssim bq \lesssim \alpha^2$ (see App. A for detailed derivation). For typical membrane properties [6], $\alpha \gtrsim 10$ is required for the approximation to be quantitatively accurate, but qualitative differences are not expected for smaller α .

The adiabatic approximation removes the time derivatives from Eqs. (3), leaving

$$\nabla^2 P_c = \nabla \cdot \mathbf{F}, \quad \text{and} \quad \Lambda_d^2 \nabla^2 \mathbf{F} - \mathbf{F} = \nabla P_{\text{act}}. \quad (5)$$

These are closed equations for the density, via P_c and P_{act} , and polarization, via \mathbf{F} , subject to the following boundary conditions (BCs): an apolar, homogeneous bulk, $\rho(z \rightarrow \infty) \rightarrow \rho_\infty$ and $\mathbf{m}(z \rightarrow \infty) \rightarrow \mathbf{0}$, and zero

normal flux at the impermeable membrane

$$\hat{\mathbf{n}} \cdot (\nabla P_c - \mathbf{F}) \Big|_{z=h} = 0 \text{ and } \hat{\mathbf{n}} \cdot (\Lambda_d^2 \nabla \mathbf{F} - P_{\text{act}}) \Big|_{z=h} = \mathbf{0}. \quad (6)$$

Consistent with Eq. (1), we aim to find $P_c(z = h)$ to first order in $|\nabla h|$ from Eqs. (5) & (6). To that end, we introduce $\xi(\mathbf{x}, z) = z - h(\mathbf{x}, t)$, measuring position above the *deformed* membrane, and the associated coordinates along it $\boldsymbol{\mu}(\mathbf{x}, z) = \mathbf{x}$ [42]. These allow BCs to be imposed at $\xi = 0$, at a cost of derivatives with respect to (\mathbf{x}, z) becoming more complicated: in the small deviation limit, we need only keep the resulting terms linear in $|\nabla h|$ [App. B Eq. (B1)]. We expand P_c and \mathbf{F} to the same order as:

$$P_c(\mathbf{x}, z) \approx P_c^{(0)}(\xi) + h(\boldsymbol{\mu}, t) \partial_\xi P_c^{(0)} + p_c(\boldsymbol{\mu}, \xi), \quad (7a)$$

$$\mathbf{F}(\mathbf{x}, z) \approx F^{(0)}(\xi) \hat{\mathbf{z}} + h(\boldsymbol{\mu}, t) \partial_\xi F^{(0)} \hat{\mathbf{z}} + \mathbf{f}(\boldsymbol{\mu}, \xi), \quad (7b)$$

where $P_c^{(0)}(z)$ and $\mathbf{F}^{(0)} = F^{(0)}(z) \hat{\mathbf{z}}$ are the solutions to Eq. (5) for $h = 0$, well established without interactions [29, 31] and found as power series near $\xi = 0$ otherwise [Eq. (B3)]. By symmetry, these depend only on z , and $\mathbf{F}^{(0)}$ only has a z -component. The first terms distort the flat-wall solutions to match the membrane profile, while p_c and \mathbf{f} are the first-order corrections needed for Eqs. (7) to satisfy Eqs. (5). Both P_{act} and P_c are functions of ρ , so their first-order corrections are related by the chain rule:

$$p_{\text{act}}(\boldsymbol{\mu}, \xi) = \frac{\dot{P}_{\text{act}}(\rho_0(\xi))}{\dot{P}_c(\rho_0(\xi))} p_c(\boldsymbol{\mu}, \xi) \equiv \chi(\xi) p_c(\boldsymbol{\mu}, \xi). \quad (8)$$

Here ρ_0 is the flat-wall density profile, which determines $\chi(\xi)$. In the non-interacting limit $\chi = \alpha^2$, allowing exact solutions [Eqs. (B10)]. With interactions, χ is a function of position, complicating our analysis.

Equations (5–8) lead to closed, linear equations for p_c and \mathbf{f} found, along with their solutions, in App. B. The solution has three independent functions (one for p_c and two for the components of \mathbf{f} parallel and perpendicular to the membrane) which, after FT in \mathbf{x} , appear with coefficients $c_1(\mathbf{q})$, $c_2(\mathbf{q})$ and $c_3(\mathbf{q})$, defined such that: $\tilde{p}_c(\mathbf{q}, \xi = 0) = c_1(\mathbf{q})$. The BCs in Eq. (6) give linear algebraic equations for c_{1-3} .

The function, $\psi(\xi)$, multiplying c_1 solves [Eqs. (B5) & (B6)]

$$\Lambda_d^2 \partial_\xi^2 \psi - (1 + \Lambda_d^2 q^2 + \chi(\xi)) \psi = 0, \quad (9)$$

with $\psi(\xi = 0) = 1$ and $\psi(\xi \rightarrow \infty) = 0$. This can be solved exactly without, but not with, interactions (App. B). However, note that Eq. (9) is a Schrödinger equation for a particle of energy $-(1 + \Lambda_d^2 q^2)$ in a potential $\chi(\xi)$. No MIPS and passive stability means $\chi(\xi) > -(1 + \Lambda_d^2 q^2)$: in quantum mechanical language, the particle is in a “classically forbidden” region and the “wavefunction”, ψ , exponentially decays.

This analogy to quantum mechanics is useful. When χ (and hence ρ_0) is slowly varying, ψ is accurately captured by the well-known Wentzel-Kramers-Brillouin (WKB) approximation [43, 44]. The difference between $\rho_0(0)$ and ρ_∞ is controlled by P_{act} in bulk $\propto \alpha^2 \rho_\infty \mathcal{V}(\rho_\infty)$. This can be large, even for moderate α , at low ρ_∞ , resulting in steep concentration gradients and a poor WKB approximation. A better approach here is to perturb around the non-interacting solution. At higher ρ_∞ , interactions reduce the bulk active pressure and flatten $\rho_0(\xi)$, improving the WKB approximation. Thus, both high and low densities are tractable.

The resulting pressure from the ABPs is,

$$\tilde{P}(\mathbf{q}, t) \approx P_c(\rho_0(0)) \delta(\mathbf{q}) + \sum_{n=1}^4 q^n X_n \tilde{h}(\mathbf{q}, t), \quad (10)$$

where the coefficients X_n can be found explicitly as functions of α and ρ_∞ (see Supplemental Material [45]). We retain terms up to q^4 , consistent with Eq. (1). The first term only affects the $q = 0$ mode and is independent of \tilde{h} . This represents the uniform pressure exerted by ABPs on the membrane, equivalent to osmotic pressure, now modified by activity. The remaining linear in \tilde{h} terms can be absorbed into an effective Hamiltonian in Eq. (1), renormalizing the apparent membrane mechanics. Specifically, X_2 and X_4 renormalize the surface tension and bending modulus respectively:

$$\gamma_{\text{eff}} = \gamma + X_2(\alpha, \rho_\infty), \quad \text{and} \quad \kappa_{\text{eff}} = \kappa + X_4(\alpha, \rho_\infty), \quad (11)$$

showing that when X_2 and/or X_4 are negative, ABPs destabilize the membrane by decreasing its effective surface tension and/or bending modulus. X_1 and X_3 encode new non-local interactions from the redistribution of ABPs along the membrane [45], absent in the standard Helfrich Hamiltonian and when the membrane interacts with an equilibrium fluid with short-range interactions [23, 24]. Without interactions, X_1 vanishes [46].

The membrane’s stability is probed by substituting Eq. (10) into Eq. (1). A mode of wavenumber q is unstable if the resulting deterministic terms on the right-hand side are positive. The instability morphology depends on which q are unstable and grow most rapidly with four qualitatively distinct possibilities: (I) a finite wavelength is most unstable with long wavelengths ($q \rightarrow 0$) also unstable; (II) same as (I) but $q \rightarrow 0$ are *stable*; (III) short wavelengths ($q \rightarrow \infty$) are the most unstable, dominating other instabilities; (IV) both long and short wavelengths unstable, but possibly a small finite range of stable wavelengths. The new X_1 and X_3 terms enable type II instabilities where a finite wavelength grows over all others, akin to Turing patterns [47] or modulated lipid domains and curvature in bilayer membranes [48].

Figure 1 maps the predicted membrane instabilities as a function of ABP density, expressed as the reduced bulk volume fraction, $\phi_\infty/\phi_{\text{max}}$, and activity in $d = 3$. The equations of state, $P_c(\rho)$ and $P_{\text{act}}(\rho)$, and $\phi_{\text{max}} = 0.645$ are taken from hard-sphere ABP simulations [34, 49]. To

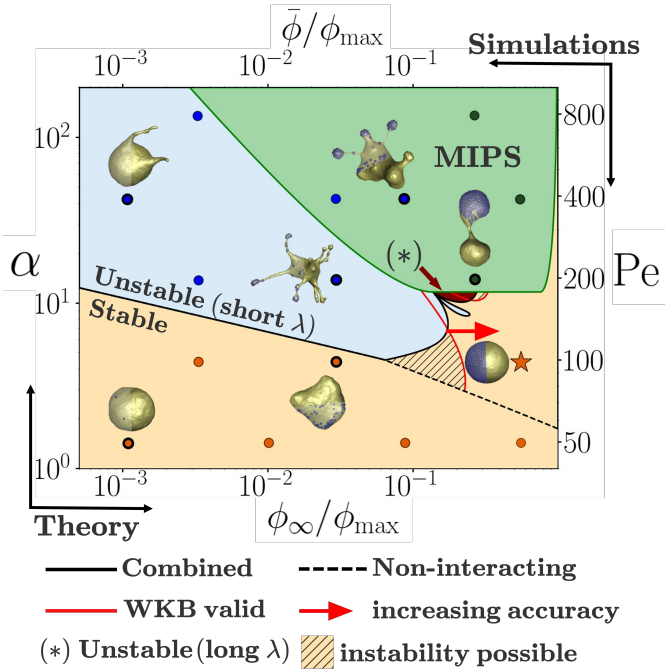


FIG. 1. *Theory (left axes):* Stability boundaries as functions of ϕ_∞/ϕ_{\max} and α in $d = 3$. Colors denote stable (orange), short-wavelength (λ) unstable (blue), long λ unstable (red), and MIPS (green) regimes. The solid black line is the non-interacting stability boundary at low ϕ_∞ , replaced by the interacting (WKB) prediction, accurate beyond the red curve, when they cross at higher ϕ_∞ ; the non-interacting line continues dashed. In the hashed region, the WKB approximation is unreliable. *Simulations (right axes):* Results from Ref. [6] shown versus $\bar{\phi}/\phi_{\max}$ and Pe . Points (outlined for snapshots) colored as in [6]: orange (“fluctuating”), blue (“tethering”), and green (“bola”). Two sets of axes allow qualitative comparison, since ϕ_∞ and $\bar{\phi}$ are not related directly.

compare with the ABP-laden spherical vesicle simulations of Vutukuri et al. [6], we match their membrane parameters. They considered relatively small (radius of $8b$) vesicles whose closed geometry means that ABP conservation is important: bulk density is ill-defined so they report overall ABP volume fraction, $\bar{\phi}$. Since our theory for an infinite membrane doesn't quantitatively apply to small vesicles, we plot the simulation data on their own axes for *qualitative* comparison. In simulations, ABP activity is measured by the Péclet number $\text{Pe} = v_0 b / D_T$.

The features of the theoretical and simulation stability maps agree excellently. In particular, at low volume fractions and activities, both show the membrane is stable and that increasing the activity here produces short wavelength instabilities (type III): the shortest wavelengths described by the theory are unstable, and simulations show long tendrils a few particle radii wide.

For low ϕ_∞/ϕ_{\max} , the non-interacting solution is expected to be accurate and provides the (solid black) stability boundary, while the WKB approximation is poor. At higher ϕ_∞ , interactions are essential and WKB deter-

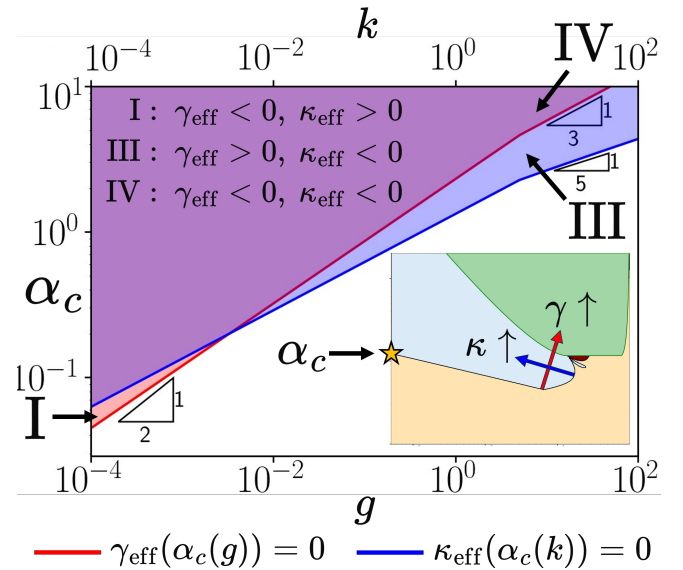


FIG. 2. Critical activity α_c at which $\gamma_{\text{eff}} = 0$ (red), or $\kappa_{\text{eff}} = 0$ (blue), plotted versus $g = \gamma V_d(b) / (\Lambda_d k_B T)$ and $k = \kappa V_d(b) / (\Lambda_d^3 k_B T)$ respectively, computed in the non-interacting limit at $\phi_\infty/\phi_{\max} = 0.05$. Scalings of α_c at large and small g and k are indicated. The yellow star (inset) marks α_c , the critical point where increasing activity destabilizes the membrane at low density to the instability type indicated in the main panel. When interactions are included, the short-wavelength unstable region (blue - inset) shrinks as γ (red arrow) or κ increase (blue arrow).

mines the stability boundary; the non-interacting solution continues as a dashed line. The WKB approximation is valid to the right of the red line; the hashed region is where the WKB solution predicts stability, but its accuracy is uncertain. Crucially, the interacting solution correctly captures the stability of vesicles at high ϕ_∞ seen in simulations (orange star), where the non-interacting solution incorrectly predicts instability. Membrane stability at high ϕ_∞ is intuitive: when ABPs are trapped ($\mathcal{V}(\rho_{\max}) = 0$), they cannot destabilize the membrane.

At high activities and volume fractions, MIPS occurs, either in bulk or due to accumulation at the membrane wall [45]. While our theory is not applicable here, simulation results are consistent with phase separation driving membrane instability. Specifically, snapshots show high-density ABP clusters pushing droplets out of the lower-density vesicle or dividing it completely. Near the MIPS boundary, WKB theory predicts a small region of long-wavelength instability. This may be an artefact of the approximation, as it appears at the limit of its validity and is insensitive to membrane parameters [45], although it could also reflect genuine pre-transitional growth of long-wavelength fluctuations preceding phase separation.

The features of the stability diagram in Fig. 1 depend on the bare membrane parameters, as expressed in Eqs. (11). The Supplemental Material shows diagrams for a range of γ and κ but the main trends are captured

by the non-interacting limit [45]. There, X_1 vanishes, so the instability type is set by the signs of γ_{eff} and κ_{eff} : (I) only $\gamma_{\text{eff}} < 0$, (III) only $\kappa_{\text{eff}} < 0$, and (IV) both negative.

Let α_c^γ and α_c^κ be the values of α satisfying $\gamma_{\text{eff}}(\alpha_c^\gamma) = 0$, and $\kappa_{\text{eff}}(\alpha_c^\kappa) = 0$; above these activities, the membrane is unstable. These can be determined from the solutions to Eqs. (5) & (6) in the non-interacting limit ($\chi = \alpha^2$) at fixed ρ_∞ . From Eqs. (11) α_c^γ depends only on γ , while α_c^κ depends only on κ . In Fig. 2 we plot α_c^γ (red line) and α_c^κ (blue line) at $\phi_\infty/\phi_{\text{max}} = 0.05$ as a function of the dimensionless membrane tension $g = \gamma V_d(b)/(k_B T \Lambda_d)$ and bending modulus $k = \kappa V_d(b)/(k_B T \Lambda_d^3)$ respectively, where $V_d(b)$ is d -dimensional spherical ABP volume. This shows membrane tension and/or bending modulus must be reduced sufficiently to see activity induced instabilities, consistent with experiments reporting instabilities only when membrane tension is reduced by orders of magnitude [5–7].

For membrane parameters used in Fig. 1 ($k \approx 154$, $g \approx 6$), only type III instabilities occur at low ABP densities. Figure 2 shows how these instabilities can be tuned with the bare membrane properties: reducing γ at fixed κ allows long-wavelength (type I) instabilities to appear. We can also extract useful scaling relations (shown in Fig. 2): $\alpha_c^\gamma \sim (g/\phi_\infty)^{1/3}$ for $g \gg 1$ and $\alpha_c^\kappa \sim (k/\phi_\infty)^{1/5}$ for $k \gg 1$, while in the opposite limits $\alpha_c^\gamma \sim (g/\phi_\infty)^{1/2}$ and $\alpha_c^\kappa \sim (k/\phi_\infty)^{1/2}$ (this behaviour only appears at extremely small k). The ϕ_∞ dependence follows from the linearity of X_2 and X_4 in ρ_∞ in the non-interacting limit.

Interactions mean $X_1 \neq 0$, complicating how stability depends on membrane properties. The inset of Fig. 2 shows the trends: increasing γ shifts the short-

wavelength-unstable region to higher α and ϕ_∞ , while increasing κ shifts it to higher α but *lower* ϕ_∞ . In App. C we quantify this by plotting where the interacting stability boundary departs from the non-interacting one as a function of bare membrane parameters.

We have developed a theory for a passive membrane interacting with ABPs, yielding a stability diagram that captures the behavior seen in simulations and experiments across ABP density and activity. This shows how active stresses renormalize the membrane's surface tension and bending modulus, and generate long-range couplings along it. Changes in membrane tension regulate important cellular processes: for example, a reduction in membrane tension in mouse embryonic stem cell development promotes endocytosis and drives early differentiation [50, 51]. Our work shows how membrane mechanics are altered by its interactions with active suspensions, not just by the membrane's physical properties (composition, chemistry etc). This provides a direct physical route by which intra- or extracellular activity can modulate membrane tension, offering insight into the mechanics of these tension-dependent processes. Extending our framework beyond the adiabatic and deterministic limits, particularly in the MIPS regime, offers a path toward a unified, multi-scale theory of active-matter-driven membranes.

Acknowledgments - This work is supported by the U.S. Department of Energy, Office of Science, Office of Basic Energy Sciences, Materials Sciences and Engineering Division under Contract No. DE-AC02-05-CH11231 within the Adaptive Interfacial Assemblies Towards Structuring Liquids program (KCTR16).

[1] R. C. May and L. M. Machesky, Phagocytosis and the actin cytoskeleton, *Journal of Cell Science* **114**, 1061 (2001).

[2] T. D. Pollard and J. A. Cooper, Actin, a central player in cell shape and movement, *Science* **326**, 1208 (2009).

[3] K. Rottner and M. Schaks, Assembling actin filaments for protrusion, *Current Opinion in Cell Biology* **56**, 53 (2019).

[4] E. S. Welf, C. E. Miles, J. Huh, E. Sapoznik, J. Chi, M. K. Driscoll, T. Isogai, J. Noh, A. D. Weems, T. Pohlkamp, K. Dean, R. Fiolka, A. Mogilner, and G. Danuser, Actin-membrane release initiates cell protrusions, *Developmental Cell* **55**, 723 (2020).

[5] S. C. Takatori and A. Sahu, Active contact forces drive nonequilibrium fluctuations in membrane vesicles, *Physical Review Letters* **124**, 158102 (2020).

[6] H. R. Vutukuri, M. Hoore, C. Abaurrea-Velasco, L. van Buren, A. Dutto, T. Auth, D. A. Fedosov, G. Gompper, and J. Vermant, Active particles induce large shape deformations in giant lipid vesicles, *Nature* **586**, 52 (2020).

[7] P. Y. Kim, S. Zhu, J. Forth, G. Xie, D. A. King, B. A. Helms, P. D. Ashby, A. K. Omar, and T. P. Russell, Shape-evolving structured liquids, *Advanced Materials* **37** (2025).

[8] A. Sahu, R. A. Sauer, and K. K. Mandadapu, Irreversible thermodynamics of curved lipid membranes, *Physical Review E* **96**, 042409 (2017).

[9] A. Sahu, A. Glisman, J. Tchoufag, and K. K. Mandadapu, Geometry and dynamics of lipid membranes: The scriven-love number, *Physical Review E* **101**, 052401 (2020).

[10] R. D. Kamien, The geometry of soft materials: a primer, *Reviews of Modern Physics* **74**, 953 (2002).

[11] R. Granek, From semi-flexible polymers to membranes: Anomalous diffusion and reptation, *Journal de Physique II* **7**, 1761 (1997).

[12] J. Happel and H. Brenner, *Low Reynolds number hydrodynamics*, Vol. 1 (Springer Netherlands, 1983).

[13] S. Kim and S. J. Karrila, *Microhydrodynamics : principles and selected applications* (Dover Publications, 2005).

[14] M. Doi and S. F. Edwards, *The theory of polymer dynamics* (Oxford University Press, 1986).

[15] Hydrodynamic interactions between the ABPs and the membrane can be approximately incorporated via an effective medium theory renormalizing \tilde{M} [52–54].

[16] W. Helfrich, Elastic properties of lipid bilayers: Theory and possible experiments, *Zeitschrift für Naturforschung C* **28**, 693 (1973).

[17] P. Canham, The minimum energy of bending as a possible explanation of the biconcave shape of the human red

blood cell, *Journal of Theoretical Biology* **26**, 61 (1970).

[18] Generally, for finite-ranged interactions (e.g. electrostatic), P must be determined by integrating over the entire suspension domain [55].

[19] M. E. Fisher, Interfaces: fluctuations, interactions and related transitions, in *Statistical Mechanics of Membranes and Surfaces*, edited by D. Nelson, T. Piran, and S. Weinberg (World Scientific, 2004) pp. 19–47.

[20] R. D. Kamien, Entropic attraction and ordering, in *Soft Matter*, edited by G. Gompper and M. Schick (Wiley, 2007) pp. 1–40.

[21] A. D. Dinsmore, A. G. Yodh, and D. J. Pine, Entropic control of particle motion using passive surface microstructures, *Nature* **383**, 239 (1996).

[22] P. D. Kaplan, J. L. Rouke, A. G. Yodh, and D. J. Pine, Entropically driven surface phase separation in binary colloidal mixtures, *Physical Review Letters* **72**, 582 (1994).

[23] E. M. Blokhuis, Existence of a bending rigidity for a hard-sphere liquid near a curved hard wall: Validity of the hadwiger theorem, *Physical Review E* **87**, 022401 (2013).

[24] I. Urrutia, Bending rigidity and higher-order curvature terms for the hard-sphere fluid near a curved wall, *Physical Review E* **89**, 032122 (2014).

[25] H. H. Wensink and H. Löwen, Aggregation of self-propelled colloidal rods near confining walls, *Physical Review E* **78**, 031409 (2008).

[26] J. Elgeti and G. Gompper, Wall accumulation of self-propelled spheres, *EPL (Europhysics Letters)* **101**, 48003 (2013).

[27] C. F. Lee, Active particles under confinement: aggregation at the wall and gradient formation inside a channel, *New Journal of Physics* **15**, 055007 (2013).

[28] B. Ezhilan, R. Alonso-Matilla, and D. Saintillan, On the distribution and swim pressure of run-and-tumble particles in confinement, *Journal of Fluid Mechanics* **781**, R4 (2015).

[29] W. Yan and J. F. Brady, The force on a boundary in active matter, *Journal of Fluid Mechanics* **785**, R1 (2015).

[30] W. Yan and J. F. Brady, The curved kinetic boundary layer of active matter, *Soft Matter* **14**, 279 (2018).

[31] A. Duzgun and J. V. Selinger, Active brownian particles near straight or curved walls: Pressure and boundary layers, *Physical Review E* **97**, 032606 (2018).

[32] O. Granek, Y. Kafri, M. Kardar, S. Ro, J. Tailleur, and A. Solon, Colloquium: Inclusions, boundaries, and disorder in scalar active matter, *Reviews of Modern Physics* **96**, 031003 (2024).

[33] N. Nikola, A. P. Solon, Y. Kafri, M. Kardar, J. Tailleur, and R. Voituriez, Active particles with soft and curved walls: Equation of state, ratchets, and instabilities, *Physical Review Letters* **117**, 098001 (2016).

[34] A. K. Omar, H. Row, S. A. Mallory, and J. F. Brady, Mechanical theory of nonequilibrium coexistence and motility-induced phase separation, *Proceedings of the National Academy of Sciences* **120** (2023).

[35] W. Yan and J. F. Brady, The swim force as a body force, *Soft Matter* **11**, 6235 (2015).

[36] J. M. Epstein, K. Klymko, and K. K. Mandadapu, Statistical mechanics of transport processes in active fluids. ii. equations of hydrodynamics for active brownian particles, *The Journal of Chemical Physics* **150** (2019).

[37] A. K. Omar, Z.-G. Wang, and J. F. Brady, Microscopic origins of the swim pressure and the anomalous surface tension of active matter, *Physical Review E* **101**, 012604 (2020).

[38] S. A. Mallory, A. K. Omar, and J. F. Brady, Dynamic overlap concentration scale of active colloids, *Physical Review E* **104**, 044612 (2021).

[39] S. C. Takatori, W. Yan, and J. F. Brady, Swim pressure: Stress generation in active matter, *Physical Review Letters* **113**, 028103 (2014).

[40] M. E. Cates and J. Tailleur, Motility-induced phase separation, *Annual Review of Condensed Matter Physics* **6**, 219 (2015).

[41] Similarly, the passive suspension ($\alpha = 0$) must be stable, i.e. $\dot{P}_c(\rho) \geq 0$.

[42] Despite appearances, these are essential: derivatives holding z and a component of \mathbf{x} constant are different from those holding ξ and the corresponding component of $\boldsymbol{\mu}$ fixed.

[43] C. M. Bender and S. A. Orszag, *Advanced Mathematical Methods for Scientists and Engineers* (McGraw-Hill Book Company, 1978).

[44] R. B. Dingle, *Asymptotic Expansions: Their Derivation and Interpretation* (Academic Press, 1973).

[45] See supplemental material for details.

[46] Note that the q^0 term is *always* absent: $c_1(q = 0)$ exactly cancels the contribution from the second term in Eq. (7a).

[47] P. K. Maini and T. E. Woolley, The turing model for biological pattern formation, in *The Dynamics of Biological Systems*, edited by A. Bianchi, T. Hillen, M. Lewis, and Y. Yi (Springer, Cham, 2019) pp. 189–204.

[48] Q. Yu and A. Košmrlj, Pattern formation of lipid domains in bilayer membranes, *Soft Matter* **21**, 4288 (2025).

[49] A. K. Omar, K. Klymko, T. GrandPre, and P. L. Geissler, Phase diagram of active brownian spheres: Crystallization and the metastability of motility-induced phase separation, *Physical Review Letters* **126**, 188002 (2021).

[50] M. Bergert, S. Lembo, S. Sharma, L. Russo, D. Milovanović, K. H. Gretarsson, M. Börmel, P. A. Neveu, J. A. Hackett, E. Petsalaki, and A. Diz-Muñoz, Cell surface mechanics gate embryonic stem cell differentiation, *Cell Stem Cell* **28**, 209 (2021).

[51] H. D. Belly, A. Stubb, A. Yanagida, C. Labouesse, P. H. Jones, E. K. Paluch, and K. J. Chalut, Membrane tension gates erk-mediated regulation of pluripotent cell fate, *Cell Stem Cell* **28**, 273 (2021).

[52] S. F. Edwards and K. F. Freed, Theory of the dynamical viscosity of polymer solutions, *The Journal of Chemical Physics* **61**, 1189 (1974).

[53] K. F. Freed and S. F. Edwards, Polymer viscosity in concentrated solutions, *The Journal of Chemical Physics* **61**, 3626 (1974).

[54] E. S. G. Shaqfeh and G. H. Fredrickson, The hydrodynamic stress in a suspension of rods, *Physics of Fluids A: Fluid Dynamics* **2**, 7 (1990).

[55] D. Henderson, An exact formula for the contact value of the density profile of a system of charged hard spheres near a charged wall, *Journal of Electroanalytical Chemistry* **102**, 315 (1979).

[56] E. C. Aifantis and J. B. Serrin, Equilibrium solutions in the mechanical theory of fluid microstructures, *Journal of Colloid and Interface Science* **96**, 530 (1983).

[57] E. C. Aifantis and J. B. Serrin, The mechanical theory of fluid interfaces and maxwell's rule, *Journal of Colloid and Interface Science* **96**, 517 (1983).

Appendix A: Separation of Timescales

Consider a perturbation to a uniform density and polarization state *along the membrane*, i.e. $\rho = \rho_0 + \delta\rho(\mathbf{x}, t)$ and $\mathbf{F} = \mathbf{F}_0 + \delta\mathbf{F}(\mathbf{x}, t)$. Linearizing Eqns. (3) in the perturbations and assuming they relax $\sim e^{-t/\tau_\rho}$, we find (in FT):

$$\frac{T_d}{\tau_\rho} \begin{pmatrix} \tilde{\delta\rho} \\ \tilde{\delta\mathbf{F}}_\parallel \end{pmatrix} = \begin{pmatrix} K_c \Lambda_d^2 q^2 / k_B T & i\mathbf{q} \Lambda_d^2 / k_B T \\ i\mathbf{q} K_{\text{act}} & (\Lambda_d^2 q^2 + 1) \end{pmatrix} \begin{pmatrix} \tilde{\delta\rho} \\ \tilde{\delta\mathbf{F}}_\parallel \end{pmatrix} \quad (\text{A1})$$

where $T_d = \tau_r/(d-1)$, $K_{c/\text{act}} = \dot{P}_{c/\text{act}}(\rho_0)$ and $\delta\mathbf{F}_\parallel$ is the component of the polarization perturbation parallel to the membrane (it is easy to show that the perpendicular component relaxes quickly, at a rate $= (\Lambda_d^2 q^2 + 1) T_d^{-1}$). The density relaxation rate is therefore controlled by the *smallest* eigenvalue of the matrix on the right hand side. In the limit $\Lambda_d q \ll 1$, this is

$$T_d \tau_\rho^{-1} \approx (K_c + K_{\text{act}})(\Lambda_d q)^2 / k_B T. \quad (\text{A2})$$

Throughout this work, we consider the case that MIPS does not occur so that the first bracket on the right hand side is always positive. MIPS occurs at high densities and activities, thus we should restrict our attention to relatively low densities where this bracket is $\approx (1 + \alpha^2)$.

The relaxation rate, τ_h^{-1} , of a membrane perturbation with wavenumber q is found from Eq. (1) in $d = 3$ to be:

$$T_d \tau_h^{-1} = 3g(\Lambda_d q) + 3k(\Lambda_d q)^3/4. \quad (\text{A3})$$

For the adiabatic approximation to hold, the ABP density must relax faster than h , i.e. $\tau_\rho^{-1} > \tau_h^{-1}$. Thus, we conclude that the adiabatic approximation can only be accurate if $\alpha^2 \gtrsim 3\sqrt{gk} - 1$ and it describes wavenumbers $g/(1 + \alpha^2) \lesssim \Lambda_d q \lesssim (1 + \alpha^2)/k$. The first condition means $\alpha \gg 1$, for typical membrane properties, $10^0 \lesssim g \lesssim 10^1$ and $10^1 \lesssim k \lesssim 10^2$. This gives the rough approximations quoted in the main text.

Appendix B: Solution Details

In the (μ, ξ) coordinates introduced in the main text, after applying the multivariable chain rule, the gradient of a scalar function is

$$\nabla f = \partial_\xi f \hat{\mathbf{z}} + \nabla_\mu f - \nabla_\mu h \partial_\xi f, \quad (\text{B1})$$

where $\nabla_\mu f = (\partial_{\mathbf{x}} f)_\xi$, is the gradient along the membrane while keeping ξ constant, *rather than* z . We use this to write Eqs. (5) to linear order in ∇h before taking the expansions in Eqs. (7).

The first order corrections to the conservative and active pressures are linked by their shared dependence on the density profile, $\rho(\mu, \xi)$. Let $\rho_0(\xi)$ be the flat wall density profile and $\rho_1(\mu, \xi)$ its first order correction. The conservative (or active) pressure outside the deformed membrane must be: $P_c(\rho_0 + \rho_1) = P_c(\rho_0) + \dot{P}_c(\rho_0)\rho_1$,

where a dot is a ρ derivative. The first term here is, by definition, $P_c^{(0)}$ and the second includes ρ_1 (along with the second term on the left hand side of Eq. (7b)). Expanding P_{act} as above, gives ρ_1 in terms of *either* ρ_0 or P_{act} . Both must be equal, and we obtain Eq. (8).

Let us provide some useful general results for the flat wall solutions. It is straightforward to show that, $F^{(0)}(\xi) = \partial_\xi P_c^{(0)}$ and hence

$$\Lambda_d^2 \partial_\xi^2 P_c^{(0)} - (P_c^{(0)} + P_{\text{act}}^{(0)} - P_c^{(0)}(0)) = 0. \quad (\text{B2})$$

This equation, paired with the boundary conditions $P_c(\xi \rightarrow \infty) = P_c(\rho_\infty)$ and $\lim_{\xi \rightarrow 0} (\Lambda_d^2 \partial_\xi^2 P_c^{(0)} - P_{\text{act}}^{(0)}) = 0$ allows $P_c^{(0)}$ to be found as a series near $\xi = 0$ easily, under the assumptions of no MIPS and repulsive interactions (i.e. $\dot{P}_c(\rho) > 0$). For our purposes the first two terms, $P_c^0 = P_c^{(0)}(0) + \xi P_c^{(1)} + \dots$, are sufficient and the coefficients are given by:

$$P_c^{(0)}(0) = P_c(\rho_\infty) + P_{\text{act}}(\rho_\infty) \equiv P_c(\rho_0(0)), \quad (\text{B3a})$$

$$\frac{1}{2} \left(\Lambda_d P_c^{(1)} \right)^2 = \int_{P_c(\rho_\infty)}^{P_c^{(0)}(0)} dP_c \left(P_c + P_{\text{act}}(P_c) - P_c^{(0)}(0) \right). \quad (\text{B3b})$$

The first of these is well-known [31, 37, 39] and establishes the density at a flat membrane $\rho_0(0)$ while the second may be found using a simple modification of the method of Aifantis and Serrin [34, 56, 57].

We find that p_c and \mathbf{f} solve (in FT):

$$\partial_\xi^2 \tilde{p}_c - q^2 \tilde{p}_c = \partial_\xi \tilde{f}_z + i\mathbf{q} \cdot \tilde{\mathbf{f}}_\parallel, \quad (\text{B4a})$$

$$\Lambda_d^2 \partial_\xi^2 \tilde{f}_z - (1 + \Lambda_d^2 q^2) \tilde{f}_z = \partial_\xi (\chi(\xi) \tilde{p}_c), \quad (\text{B4b})$$

$$\Lambda_d^2 \partial_\xi^2 \tilde{\mathbf{f}}_\parallel - (1 + \Lambda_d^2 q^2) \tilde{\mathbf{f}}_\parallel = i\mathbf{q} \chi(\xi) \tilde{p}_c, \quad (\text{B4c})$$

where f_z and \mathbf{f}_\parallel are the components of the polarization perpendicular and parallel to the flat membrane respectively. We construct the solutions for \tilde{p}_c and $\tilde{\mathbf{f}}$ that vanish as $\xi \rightarrow \infty$ as follows:

$$\tilde{p}_c(\mathbf{q}, \xi) = c_1 \psi(\xi) + c_2 \varphi(\xi), \quad (\text{B5})$$

where ψ and φ solve,

$$\Lambda_d^2 \psi''(\xi) - (1 + \Lambda_d^2 q^2 + \chi(\xi)) \psi(\xi) = 0, \quad (\text{B6a})$$

subject to $\psi(\xi = 0) = 1$ and $\psi(\xi \rightarrow \infty) = 0$ and,

$$\Lambda_d^2 \varphi''(\xi) - (1 + \Lambda_d^2 q^2 + \chi(\xi)) \varphi(\xi) = e^{-q\xi}, \quad (\text{B6b})$$

such that $\varphi(\xi = 0) = 0$ and $\varphi(\xi \rightarrow \infty) \rightarrow 0$.

$$\begin{aligned} \tilde{\mathbf{f}}_\parallel(\mathbf{q}, \xi) &\equiv i\mathbf{q} \tilde{f}_\parallel(\mathbf{q}, \xi) \\ &= i\mathbf{q} \left[\tilde{p}_c(\mathbf{q}, \xi) + c_2 e^{-q\xi} - c_3 q^{-2} \lambda(q) e^{-\lambda(q)\xi} \right], \end{aligned} \quad (\text{B7})$$

$$\tilde{f}_z(\mathbf{q}, \xi) = \tilde{f}'_{\parallel}(\mathbf{q}, \xi) - c_3(\Lambda_d q)^{-2} e^{-\lambda(q)\xi}, \quad (\text{B8})$$

where $\lambda(q) = \sqrt{\Lambda_d^{-2} + q^2}$.

The constants, c_1 , c_2 and c_3 , are found by matching the BCs in Eq. (6) at $\xi = 0$.

$$qc_2 - c_3 = 0, \quad (\text{B9a})$$

$$\lambda^2(q)(c_1 + c_2) - \lambda(q)c_3 = -\Lambda_d^{-2}h(\mathbf{q}, t)P_c^{(1)}, \quad (\text{B9b})$$

$$\mathcal{J}(q^2)c_1 + [\mathcal{K}(q) - q]c_2 + c_3(\lambda(q)/q)^2 = -\Lambda_d^{-2}h(\mathbf{q}, t)P_{\text{act}}^0. \quad (\text{B9c})$$

Here, we have defined $P_{\text{act}}^0 \equiv P_{\text{act}}(\rho_0(0))$, as well as $\mathcal{J}(q^2) = \psi'(\xi = 0)$ and $\mathcal{K}(q) = \varphi'(\xi = 0)$.

In the non-interacting limit, $\chi = \alpha^2$, and we find

$$\psi(\xi) = e^{-\lambda_{\alpha}(q)\xi}, \quad \text{and} \quad \varphi(\xi) = \frac{e^{-\lambda_{\alpha}(q)\xi} - e^{-q\xi}}{1 + \alpha^2}, \quad (\text{B10})$$

where we have defined $\lambda_{\alpha}(q) = \sqrt{\lambda^2(q) + (\alpha/\Lambda_d)^2}$. Using the well-known flat wall solutions [29] for non-interacting ABPs, we find the coefficients of Eq. (10)

$$X_2 = -k_B T \Lambda_d \rho_{\infty} \alpha^2 \sqrt{1 + \alpha^2}, \quad (\text{B11a})$$

$$X_3 = k_B T \Lambda_d^2 \rho_{\infty} \alpha^2 (1 + 2\alpha^2)/2, \quad (\text{B11b})$$

$$X_4 = -\frac{k_B T \Lambda_d^3 \rho_{\infty} \alpha^2}{2(1 + \alpha^2)} \left(d(\alpha) + (2\alpha^2 + 1)\sqrt{1 + \alpha^2} \right), \quad (\text{B11c})$$

where $d(\alpha) = 2\alpha^4 - \alpha^2 - 2$. These expressions provide expressions for γ_{eff} and κ_{eff} .

In the interacting case, we use WKB approximations for ψ and φ [43, 44]:

$$\psi(\xi) \approx \left(\frac{Q(\mathbf{q}, 0)}{Q(\mathbf{q}, \xi)} \right)^{1/4} \exp \left(-\frac{1}{\Lambda_d} \int_0^{\xi} d\xi' \sqrt{Q(\mathbf{q}, \xi')} \right), \quad (\text{B12a})$$

$$\varphi(\xi) = \int_0^{\infty} d\xi' G_Q(\xi, \xi') e^{-q\xi'}, \quad (\text{B12b})$$

where $Q(\mathbf{q}, \xi) = (1 + \Lambda_d^2 q^2 + \chi(\xi))$ and G_Q is the required Green function for Eq. (B6b) (see Sec. 10.3 of [43]). Since φ is expressed as an integral, $\mathcal{K}(q)$ shall be also, which can be approximated as a series in powers of derivatives of χ [45]. Concrete expressions for $X_{1 \rightarrow 4}$ are found in the Supplemental Material [45].

Appendix C: Changing membrane properties

Figure 3 illustrates the dependencies of key features of the stability diagram on the membrane properties.

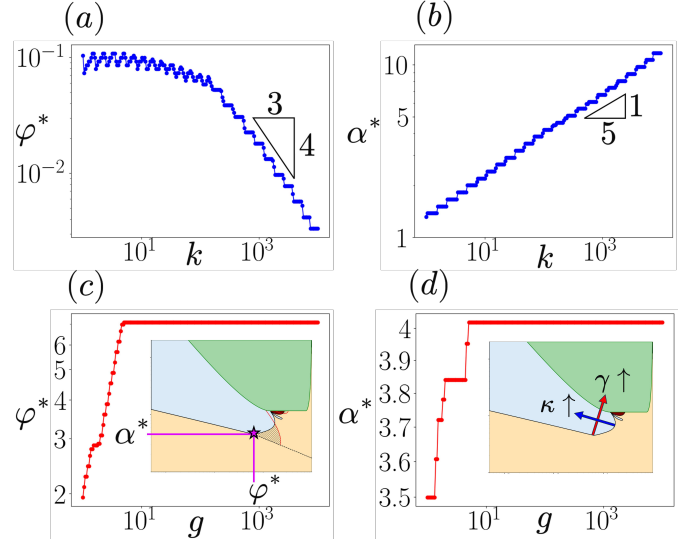


FIG. 3. Plots of the reduced volume fraction, φ^* [(a) and (c)], and activity, α^* [(b) and (d)], where the interacting solution departs from the non-interacting solution [pink star, inset panel (c)] as functions of reduced bending modulus, k panels (a) and (b), and surface tension, g panels (c) and (d). Approximate scalings with k are indicated. When held fixed, membrane parameters are $g = 6$ and $k = 154$, consistent with those in Fig. 1. These show how the blue region of short wavelength instability shrinks when γ or κ are increased, as shown by the red and blue arrows in the inset of panel (d).

Supplemental Material: Active Particle Destabilize Passive Membranes

David A. King,^{1, 2, *} Thomas P. Russell,^{3, 1} and Ahmad K. Omar^{1, 2, †}

¹*Materials Science Division, Lawrence Berkeley National Laboratory, Berkeley CA 94720.*

²*Department of Materials Science and Engineering, University of California, Berkeley, CA 94720.*

³*Polymer Science and Engineering Department, University of Massachusetts, Amherst MA 01003.*

CONTENTS

I. Expressions for $X_{1 \rightarrow 4}$ with interactions	1
A. Approximating $\mathcal{J}(q^2)$	2
B. Approximating $\mathcal{K}(q)$	2
C. Final expressions	3
II. Origins of the effective non-local terms	3
A. General Argument	4
B. Non-interacting case	4
III. Changing Membrane Properties	5
IV. Details of Motility Induced Phase Separation Spinodal	5
References	6

I. EXPRESSIONS FOR $X_{1 \rightarrow 4}$ WITH INTERACTIONS

In this section, we provide the expressions for the coefficients $X_{1 \rightarrow 4}$ appearing in Eq. (10) of the main text. The non-interacting case was handled in the main appendix. Here we focus on the interacting case, and provide some additional details about their derivation. Our starting points are Eqs. (B9) of the main text:

$$qc_2(\mathbf{q}) - c_3(\mathbf{q}) = 0, \quad (1a)$$

$$\lambda^2(q)(c_1(\mathbf{q}) + c_2(\mathbf{q})) - \lambda(q)c_3(\mathbf{q}) = -\Lambda_d^{-2}h(\mathbf{q}, t)P_c^{(1)}, \quad (1b)$$

$$\mathcal{J}(q^2)c_1(\mathbf{q}) + [\mathcal{K}(q) - q]c_2(\mathbf{q}) + c_3(\mathbf{q})(\lambda(q)/q)^2 = -\Lambda_d^{-2}h(\mathbf{q}, t)P_{\text{act}}^0. \quad (1c)$$

Here, we have defined $\lambda(q) = \sqrt{\Lambda_d^{-2} + q^2}$, $P_{\text{act}}^0 \equiv P_{\text{act}}(\rho_0(0))$, as well as $\mathcal{J}(q^2) = \psi'(\xi = 0)$ and $\mathcal{K}(q) = \varphi'(\xi = 0)$. Recall that primes denote differentiation with respect to ξ . From these expressions we find $c_1(\mathbf{q})$ which is then expanded to fourth order in q as:

$$c_1(\mathbf{q}) \approx X_1q + X_2q^2 + X_3q^3 + X_4q^4 + \dots \quad (2)$$

In order to find $X_{1 \rightarrow 4}$, therefore, we need expressions for $\mathcal{J}(q^2)$ and $\mathcal{K}(q)$. Let us handle each in turn.

* daking2@lbl.gov

† aomar@berkeley.edu

A. Approximating $\mathcal{J}(q^2)$

By definition $\mathcal{J}(q^2) = \psi'(\xi = 0)$ and Eq. (9) of the main text shows that ψ solves

$$\Lambda_d^2 \psi''(\xi) - (1 + \Lambda_d^2 q^2 + \chi(\xi)) \psi(\xi) = 0 \quad (3)$$

with boundary conditions $\psi(0) = 1$ and $\psi(\infty) = 0$. As discussed in the main text, at moderate activities and high densities, the solution can be approximated using WKB theory [1].

$$\psi(\xi) \approx \left(\frac{Q(\mathbf{q}, 0)}{Q(\mathbf{q}, \xi)} \right)^{1/4} \exp \left(-\frac{1}{\Lambda_d} \int_0^\xi d\xi' \sqrt{Q(\mathbf{q}, \xi')} \right), \quad (4)$$

where $Q(\mathbf{q}, \xi) = (1 + \Lambda_d^2 q^2 + \chi(\xi))$. Direct differentiation of this yields

$$\mathcal{J}(q^2) \approx -\sqrt{Q(0)} \left(1 + \frac{Q'(0)}{4Q^{3/2}(0)} \right) = -\sqrt{1 + q^2 + \chi(0)} \left(1 + \frac{\chi'(0)}{4(1 + q^2 + \chi(0))^{3/2}} \right). \quad (5)$$

Notice that $\chi'(0)$ appears in this expression. It is not immediately obvious that this can be expressed in terms of quantities introduced in the main text and appendices, but a few applications of the chain rule clears this up.

$$\chi'(0) = \lim_{\xi \rightarrow 0} \frac{d}{d\xi} \frac{\dot{P}_{\text{act}}(\rho_0(\xi))}{\dot{P}_{\text{c}}(\rho_0(\xi))} = \frac{\dot{P}_{\text{act}}(\rho_0(0))}{\dot{P}_{\text{c}}(\rho_0(0))} \left[\frac{\ddot{P}_{\text{act}}(\rho_0(0))}{\dot{P}_{\text{act}}(\rho_0(0))} - \frac{\ddot{P}_{\text{c}}(\rho_0(0))}{\dot{P}_{\text{c}}(\rho_0(0))} \right] \rho'_0(0), \quad (6)$$

where dots denote differentiation of the equations of stat with respect to ρ . The value of the flat wall density profile at the wall is known exactly from $P_{\text{c}}(\rho_0(0)) = P_{\text{c}}(\rho_\infty) + P_{\text{act}}(\rho_\infty)$. The value of its derivative at the wall is also known and revealed by the chain rule

$$\rho'_0(0) = \frac{P'_c(0)}{\dot{P}_c(\rho_0(0))} = \frac{P_c^{(1)}}{\dot{P}_c(\rho_0(0))} \quad (7)$$

where $P_c^{(1)}$ was found in the appendix of the main text.

B. Approximating $\mathcal{K}(q)$

To approximate $\mathcal{K}(q) = \varphi'(\xi = 0)$ along the same lines, we need to work a little harder. First, recall that $\varphi(\xi)$ is the solution to

$$\Lambda_d^2 \varphi''(\xi) - Q(\mathbf{q}, \xi) \varphi(\xi) = e^{-q\xi}, \quad (8)$$

subject to the boundary conditions $\varphi(0) = 0$ and $\varphi(\infty) = 0$. This is solved formally with a Green function, G_Q , in the usual fashion

$$\varphi(\xi) = \int_0^\infty d\xi' G_Q(\xi, \xi') e^{-q\xi'}, \quad (9)$$

where G_Q solves

$$\Lambda_d^2 \frac{d^2}{d\xi^2} G_Q(\xi, \xi') - Q(\mathbf{q}, \xi) G_Q(\xi, \xi') = \delta(\xi - \xi'). \quad (10)$$

This can also be analyzed using WKB theory [2] to obtain the standard expression

$$G_Q(\xi, \xi') = -\frac{1}{Q^{1/4}(\xi) Q^{1/4}(\xi')} \begin{cases} e^{-\frac{1}{\Lambda_d} \int_0^{\xi'} d\xi \sqrt{Q(\xi)}} \sinh \left(\frac{1}{\Lambda_d} \int_0^\xi d\xi \sqrt{Q(\xi)} \right), & \text{if } \xi < \xi' \\ \sinh \left(\frac{1}{\Lambda_d} \int_0^{\xi'} d\xi \sqrt{Q(\xi)} \right) e^{-\frac{1}{\Lambda_d} \int_0^\xi d\xi \sqrt{Q(\xi)}} & \text{if } \xi > \xi', \end{cases} \quad (11)$$

whence we obtain

$$\mathcal{K}(q) = -\frac{Q^{1/4}(0)}{\Lambda_d} \int_0^\infty d\xi e^{-q\xi} \frac{e^{-\frac{1}{\Lambda_d} \int_0^\xi d\xi \sqrt{Q(\xi)}}}{Q^{1/4}(\xi)}. \quad (12)$$

We cannot compute this integral exactly. However, we can approximate it by noting that the exponential factors in the integrand will strongly suppress any contributions away from $\xi = 0$. Therefore, we can expand the terms in the integrand as

$$Q^{-1/4}(\xi) \approx Q^{-1/4}(0) - \frac{Q'(0)}{4Q^{5/4}(0)}\xi + \mathcal{O}(\xi^2) \quad (13a)$$

and

$$\int_0^\xi d\zeta \sqrt{Q(\zeta)} \approx \sqrt{Q(0)}\xi + \frac{Q'(0)}{4\sqrt{Q(0)}}\xi^2 + \mathcal{O}(\xi^3). \quad (13b)$$

This lets us obtain the approximation

$$\mathcal{K}(q) \approx -\frac{1}{\Lambda_d q + \sqrt{Q(0)}} + \Lambda_d \frac{Q'(0)}{4Q(0)} \frac{1}{(\Lambda_d q + \sqrt{Q(0)})^2} + \dots \quad (14)$$

These are the first of a series of approximations to $\mathcal{K}(q)$, with each subsequent term including higher and higher derivatives or higher and higher powers of derivatives of Q at $\xi = 0$. Notice that this structure is *the same* as arises from the WKB approximation for $\psi(\xi)$ which leads to the approximation (5) for $\mathcal{J}(q^2)$ [2, 3]. Therefore, to the same order of accuracy of the WKB approximation, we need only keep the first two terms in the approximation for $\mathcal{K}(q)$.

C. Final expressions

Using the results above, it is tedious but straightforward to obtain:

$$X_1/\Lambda_d = P_{\text{act}}(0) - P_c^{(1)}\mathcal{J}(0) \quad (15)$$

$$X_2/\Lambda_d^2 = P_c^{(1)} [1 + \mathcal{J}(0)(1 - \mathcal{J}(0) + \mathcal{K}(0))] + P_{\text{act}}(0) [\mathcal{J}(0) - \mathcal{K}(0) - 1] \quad (16)$$

$$\begin{aligned} X_3/\Lambda_d^3 &= P_c^{(1)} [-\mathcal{J}(0)^3 + 2\mathcal{J}(0)^2(1 + \mathcal{K}(0)) - \Lambda_d\mathcal{J}_1(0) - \mathcal{J}(0)(\mathcal{K}(0)^2 + \mathcal{K}(0) - 1 - \Lambda_d\mathcal{K}_1(0))] \\ &\quad + P_{\text{act}}(0) [\mathcal{J}(0)^2 + \mathcal{K}(0) + \mathcal{K}(0)^2 - 2\mathcal{J}(0)(1 + \mathcal{K}(0)) - \Lambda_d\mathcal{K}_1(0)] \end{aligned} \quad (17)$$

$$\begin{aligned} X_4/\Lambda_d^4 &= \frac{1}{2} \left(P_{\text{act}}(0) \left(1 + 2\mathcal{J}(0)^3 - 2\mathcal{K}(0)^2 - 2\mathcal{K}(0)^3 - 6\mathcal{J}(0)^2(1 + \mathcal{K}(0)) + 2\Lambda_d\mathcal{J}_1(0) \right. \right. \\ &\quad \left. \left. + \mathcal{J}(0)(2 + 8\mathcal{K}(0) + 6\mathcal{K}(0)^2 - 4\Lambda_d\mathcal{K}_1(0)) + 2\Lambda_d\mathcal{K}_1(0) + 4\mathcal{K}(0)\Lambda_d\mathcal{K}_1(0) - \Lambda_d^2\mathcal{K}_2(0) \right) \right. \\ &\quad \left. + P_c^{(1)} \left(-2 - 2\mathcal{J}(0)^4 + 6\mathcal{J}(0)^3(1 + \mathcal{K}(0)) + 2(1 + \mathcal{K}(0))\Lambda_d\mathcal{J}_1(0) + \mathcal{J}(0)^2(-8\mathcal{K}(0) - 6\mathcal{K}(0)^2 + 4\Lambda_d\mathcal{K}_1(0)) \right. \right. \\ &\quad \left. \left. + \mathcal{J}(0)(-3 + 2\mathcal{K}(0)^2 + 2\mathcal{K}(0)^3 - 4\Lambda_d\mathcal{J}_1(0) - 2\Lambda_d\mathcal{K}_1(0) - 2\mathcal{K}(0)(1 + 2\Lambda_d\mathcal{K}_1(0)) + \Lambda_d^2\mathcal{K}_2(0)) \right) \right) \end{aligned} \quad (18)$$

In all of these expressions, subscripts denote differentiation with respect to q , i.e. $\mathcal{J}_n(0) = \lim_{q \rightarrow 0} d^n \mathcal{J}(q)/dq^n$. Equations (5) and (14) allow each of these coefficients to be computed from the quantities, $\rho_0(0)$ and $P_c^{(1)}$ which are determined by the equations of state $P_c(\rho)$ and $P_{\text{act}}(\rho)$ as well as the bulk density, ρ_∞ and activity α .

II. ORIGINS OF THE EFFECTIVE NON-LOCAL TERMS

In this section we discuss the origins of the X_1 and X_3 terms in the pressure exerted by the active particles on the membrane. These encode effective *non-local* interactions between different points on the membrane surface and are mediated by the rearrangements of the particles above. Our goal here is not to present a detailed derivation of these terms (which would essentially recapitulate the calculation in the main text) but rather provide a physical picture that shows how they arise naturally from the governing equations. As our main focus will be their functional forms, unimportant constants and signs shall generally be ignored in this section, and the symbol “ \sim ” used to mean “looks like” or “includes a term like”. We begin with a general heuristic that shows the origin of the $X_1 q$ term (recall $q = |\mathbf{q}|$ where \mathbf{q} is the wave vector of a disturbance to the flat membrane) before explaining how this should be modified in the *non-interacting case* where this term is *absent* and the first non-local term is $X_3 q^3$.

A. General Argument

As discussed in the main text, we are aiming to solve:

$$\nabla^2 P_c = \nabla \cdot \mathcal{F}, \quad \text{and} \quad \nabla^2 \mathcal{F} - \mathcal{F} = \nabla P_{\text{act}}, \quad (19)$$

for notational simplicity, here and henceforth, we non-dimensionalize lengths by the diffusion length, Λ_d , and work with reduced polarization $\mathcal{F} = \Lambda_d \mathbf{F}$. Equations (19) are coupled non-linear partial differential equations for the density, ρ , via P_c and P_{act} and the polarization, via \mathcal{F} .

It is well known that active particles will preferentially orient perpendicular to a hard wall [4–7]. Therefore, it is natural to approximate $\mathcal{F} \sim \hat{\mathbf{n}}(\mathbf{x})\delta(z)$, where $\hat{\mathbf{n}}$ is the local normal to the membrane surface, \mathbf{x} are the coordinates along it and z is the normal coordinate to the membrane. We have taken the z dependence of the polarization to be $\delta(z)$ to represent its, relatively rapid, decay to a homogeneous apolar state far from the membrane. The exact choice is not important for the argument, which is identical even when more realistic forms are used (e.g. exponential decay $\sim e^{-z/\ell_z}$), this one keeps our analysis as simple as possible. Using our approximation for \mathcal{F} in the first equation above, we have to solve

$$\nabla^2 P_c \sim \delta(z) \nabla \cdot \hat{\mathbf{n}}(\mathbf{x}) \quad (20)$$

and find Fourier transform (FT) of the pressure at the membrane, $\tilde{P}_c(\mathbf{q}, z = 0)$. Taking the full FT of both sides above, i.e. $\tilde{f}(\mathbf{q}, k) = \int d\mathbf{x} dz e^{i\mathbf{q} \cdot \mathbf{x}} e^{ikz} f(\mathbf{x}, z)$, we find

$$\tilde{P}_c(\mathbf{q}, k) \sim \frac{q^2 \tilde{h}(q)}{k^2 + q^2} \quad (21)$$

where we have expanded the normal for small membrane deviations, $\hat{\mathbf{n}} \sim \hat{\mathbf{z}} - \nabla h$ and whence the value at $z = 0$ follows

$$\tilde{P}_c(\mathbf{q}, z = 0) \sim \int_{-\infty}^{\infty} dk \frac{q^2 \tilde{h}(\mathbf{q})}{k^2 + q^2} \sim q h(q), \quad (22)$$

the integral in the last step can be evaluated using elementary methods (e.g. the residue theorem).

This reveals how effective long-range interactions along the membrane arise. A local deformation of the membrane reorients nearby active particles (as captured by the right-hand side of Eq. (20)). The resulting particle currents redistribute the particle density above and along the membrane, through the Laplacian term on the left-hand side of Eq. (20). This change in density in turn changes the pressure. As a consequence, changing the membrane curvature at one point affects the forces acting on the membrane at distant locations: the active particle suspension transmits this influence, effectively coupling remote regions of the membrane.

B. Non-interacting case

Having seen the general origin of a term $\sim X_1 q \tilde{h}$ in the pressure on the membrane, let us consider why this term is not present for non-interacting active particles. To do this, we shall use the mathematical construction of Yan and Brady [5] who considered an ideal active Brownian particle suspension outside a generally curved surface using boundary layer theory. In the absence of interactions, Eqs. (19) are simplified because $P_{\text{act}} = \alpha^2 P_c$. Upon defining $\nabla \cdot \mathcal{F} = \mathcal{G}$, it may be shown that, in this case,

$$\nabla^2 \mathcal{G} - (1 + \alpha^2) \mathcal{G} = 0. \quad (23)$$

We can use this to substitute for \mathcal{G} in the first of Eq. (19)

$$\nabla^2 P_c \sim \nabla^2 \mathcal{G} = \nabla^2 (\nabla \cdot \mathcal{F}). \quad (24)$$

Taking the same form for \mathcal{F} and applying the same argument as in the previous section, we find $\tilde{P}_c(\mathbf{q}, z = 0) \sim q^3 \tilde{h}$. To get this term and not a term linear in q it was necessary to use Eq. (23) which *only holds in the non-interacting case* when $P_c \propto P_{\text{act}}$. Without this equation, there will always be a term that behaves $\sim \nabla \cdot \mathcal{F}$ on the right hand side of the first of Eqs. (19).

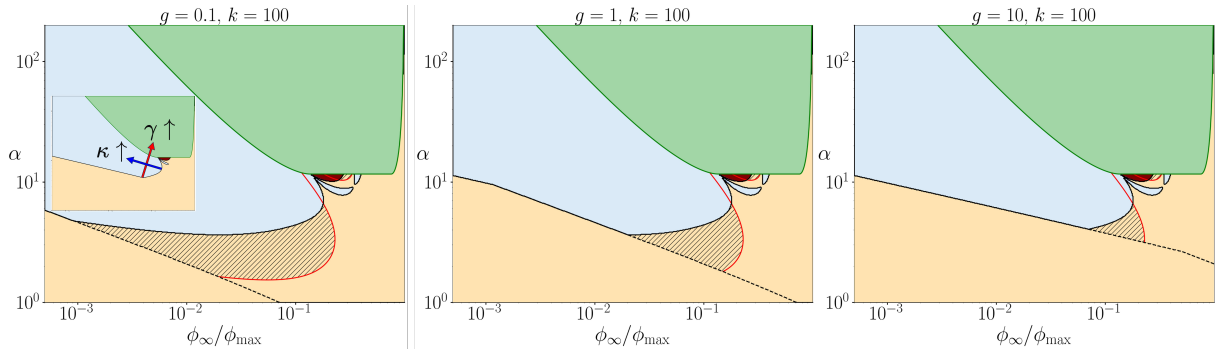


FIG. 1. Stability diagrams as a function of bulk volume fraction, ϕ_∞/ϕ_{\max} , and activity, α , for a fixed non-dimensional bare bending modulus $k = 100$ as the non-dimensional tension is varied from $g = 0.1$ to $g = 10$. The inset shows the rough direction in which the unstable region shrinks as the membrane properties change.

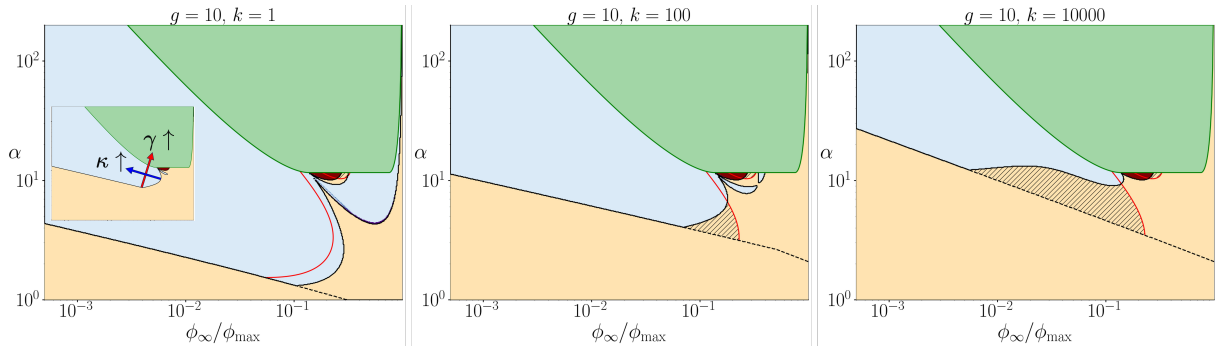


FIG. 2. Stability diagrams as a function of bulk volume fraction, ϕ_∞/ϕ_{\max} , and activity, α , for a fixed non-dimensional bare surface tension $g = 10$ as the non-dimensional bending modulus is varied from $k = 1$ to $k = 10,000$. The inset shows the rough direction in which the unstable region shrinks as the membrane properties change.

III. CHANGING MEMBRANE PROPERTIES

Here, we show how changing the the surface tension, γ , and bending modulus, κ , alters the stability map as a function of particle volume fraction ϕ_∞/ϕ_{\max} and activity α , shown in Fig. 1 of the main text. We use non-dimensionalized membrane parameters $g = \gamma V_d(b)/(\Lambda_d k_B T)$ and $k = \kappa V_d(b)/(\Lambda_d^3 k_B T)$, as in the main text.

For reference, in the simulations of Vutukuri et al. [8] referenced in the main text, these parameters take values: $g = 6$ and $k = 154$. This motivates us to choose a representative value of $k = 100$ and sweep g from 0.1 to 10 in Fig. 1. This shows that the blue region (short wavelength instability) shrinks as surface tension increase. The rough direction in which it shrinks is indicated by the red arrow in the inset. In Fig. 2, we keep $g = 10$ fixed and change k from 1 to 10,000. This shows that the short-wavelength-unstable region shrinks as k increases. Roughly speaking, the region shrinks in the direction perpendicular to that when g increases, as indicated by the red arrow in the inset.

IV. DETAILS OF MOTILITY INDUCED PHASE SEPARATION SPINODAL

To determine where motility induced phase separation (MIPS) occurs, we use the spinodal criterion, $\dot{\mathcal{P}}(\rho) = \dot{P}_c(\rho) + \dot{P}_{\text{act}}(\rho) \leq 0$ (dots denote ρ derivatives), that determines the linear stability of a homogeneous suspension to infinitessimal deviations. Finite perturbations, e.g nucleation events, can destabilize a suspension *between* the spinodal and the binodal, but we shall ignore these for simplicity.

It is not immediately obvious how to apply the spinodal criterion to the stability of an interacting suspension of active particles outside a flat wall because the density profile, ρ_0 , is not homogeneous. However, recall that if the function $Q(\mathbf{q}, \xi) = (1 + \Lambda_d^2 q^2 + \chi(\xi)) < 0$, then the perturbations to this density profile caused by membrane deformations will become oscillatory [see Eq. (4)]. Using the definition of $\chi(\xi) = \dot{P}_{\text{act}}(\rho_0(\xi))/\dot{P}_c(\rho_0(\xi))$, where ξ is the distance from the membrane, the stability of the passive suspension and the positivity of $\Lambda_d^2 q^2$, it follows that

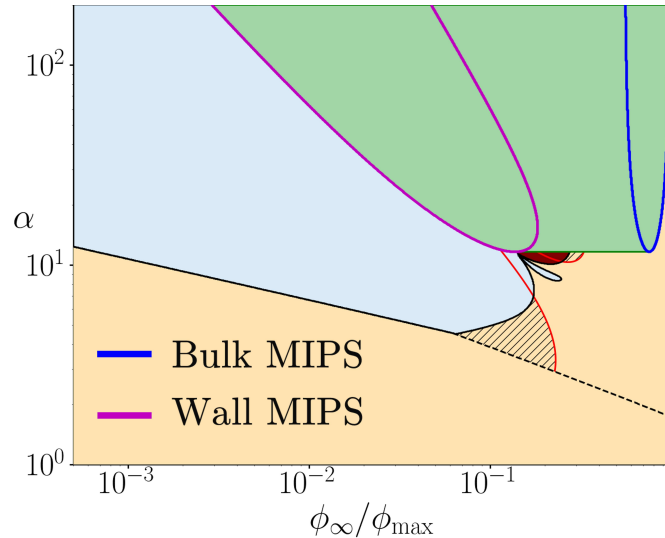


FIG. 3. Stability diagrams as a function of bulk volume fraction, ϕ_∞/ϕ_{\max} , and activity, α , for the membrane parameters used in the main text $g = 6$ and $k = 154$. The spinodals corresponding the bulk and wall densities are shown in blue and pink respectively. Given our assumptions, the flat wall density profile will reach all densities between these two values, and the composition of all of the corresponding spinodals gives the total MIPS region in green.

$Q > 0$ at a point if $\dot{\mathcal{P}}(\rho_0(\xi)) > 0$ there too. This immediately tells us that the bulk density ρ_∞ must be outside the spinodal, i.e. $\dot{\mathcal{P}}(\rho_\infty) > 0$, because if the perturbations to the flat wall density oscillate infinitely far from the membrane, then they are incompatible with a homogeneous, apolar bulk suspension. Similarly, if the flat wall profile *ever* reaches a density where $\dot{\mathcal{P}} < 0$, then our stability analysis will not hold because the oscillatory corrections would need to be delicately matched to the exponentially decaying corrections in bulk [2, 3]. This restriction implies that the flat wall density profile is strictly monotonically decreasing from the value $\rho_0(0)$ to ρ_∞ . Therefore, in order to focus only on regions where MIPS does not occur (without activated nucleation events) we restrict our attention to densities (and activities) where: $\dot{\mathcal{P}}(\rho) > 0$, $\forall \rho \in [\rho_\infty, \rho_0(0)]$.

In Fig. 3 we show how this gives rise to the extended green MIPS region in our stability map (Fig. 1 of the main text). The extremal spinodal boundaries are shown: $\dot{\mathcal{P}}(\rho_0(0)) = 0$ in pink and $\dot{\mathcal{P}}(\rho_\infty)$ in blue. The flat wall density profile at some point reaches every density between these two values, with each giving rise to a different spinodal. All of these regions are combined to give the total green MIPS region.

[1] Although, this naming convention does not appropriately apportion the credit for its discovery. For a full discussion, see [3].
[2] C. M. Bender and S. A. Orszag, *Advanced Mathematical Methods for Scientists and Engineers* (McGraw-Hill Book Company, 1978).
[3] R. B. Dingle, *Asymptotic Expansions: Their Derivation and Interpretation* (Academic Press, 1973).
[4] W. Yan and J. F. Brady, The force on a boundary in active matter, *Journal of Fluid Mechanics* **785**, R1 (2015).
[5] W. Yan and J. F. Brady, The curved kinetic boundary layer of active matter, *Soft Matter* **14**, 279 (2018).
[6] A. Duzgun and J. V. Selinger, Active brownian particles near straight or curved walls: Pressure and boundary layers, *Physical Review E* **97**, 032606 (2018).
[7] D. Saintillan and M. J. Shelley, Theory of active suspensions, in *Complex Fluids in Biological Systems*, edited by S. Spagnolie (Springer, 2015) pp. 319–355.
[8] H. R. Vutukuri, M. Hoore, C. Abaurrea-Velasco, L. van Buren, A. Dutto, T. Auth, D. A. Fedosov, G. Gompper, and J. Vermant, Active particles induce large shape deformations in giant lipid vesicles, *Nature* **586**, 52 (2020).